CHEMISTRY
A EUROPEAN JOURNAL

DOI: 10.1002/chem.201101779

Lanthanide(III) Complexes That Contain a Self-Immolative Arm: Potential Enzyme Responsive Contrast Agents for Magnetic Resonance Imaging

Thomas Chauvin,[a] Susana Torres,[b] Renato Rosseto,[b] Jan Kotek,[c] Bernard Badet,[b] Philippe Durand,*[b] and Éva Tóth*[a]

Abstract: Enzyme-responsive MRI-contrast agents containing a "self-immolative" benzylcarbamate moiety that links the MRI-reporter lanthanide complex to a specific enzyme substrate have been developed. The enzymatic cleavage initiates an electronic cascade reaction that leads to a structural change in the Ln^{III} complex, with a concomitant response in its MRI-contrast-enhancing properties. We synthesized and investigated a series of Gd^{3+} and Yb^{3+} complexes, including those bearing a self-immolative arm and a sugar unit as selective substrates for β-galactosidase; we synthesized complex **LnL^1**, its NH_2 amine derivatives formed after enzymatic cleavage, **LnL^2**, and two model compounds, **LnL^3** and **LnL^4**. All of the Gd^{3+} complexes synthesized have a single inner-sphere water molecule. The relaxivity change upon enzymatic cleavage is limited (3.68 vs. 3.15 $mM^{-1}s^{-1}$ for complexes **GdL^1** and **GdL^2**, respectively; 37 °C, 60 MHz), which prevents application of this system as an enzyme-responsive T_1 relaxation agent. Variable-temperature ^{17}O NMR spectroscopy and ^1H NMRD (nuclear magnetic relaxation dispersion) analysis were used to assess the parameters that determine proton relaxivity for the Gd^{3+} complexes, including the water-exchange rate (k_{ex}^{298}, varies in the range $1.5–3.9\times10^6\ s^{-1}$). Following the enzymatic reaction, the chelates contain an exocyclic amine that is not protonated at physiological pH, as deduced from pH-potentiometric measurements (log $K_H = 5.12(\pm0.01)$ and $5.99(\pm0.01)$ for **GdL^2** and **GdL^3**, respectively). The Yb^{3+} analogues show a PARACEST effect after enzymatic cleavage that can be exploited for the specific detection of enzymatic activity. The proton-exchange rates were determined at various pH values for the amine derivatives by using the dependency of the CEST effect on concentration, saturation time, and saturation power. A concentration-independent analysis of the saturation-power-dependency data was also applied. All these different methods showed that the exchange rate of the amine protons of the Yb^{III} complexes decreases with increasing pH value (for **YbL^3**, $k_{ex} = 1300\ s^{-1}$ at pH 8.4 vs. $6000\ s^{-1}$ at pH 6.4), thereby resulting in a diminution of the observed CEST effect.

Keywords: enzymatic detection · lanthanides · MRI contrast agents · PARACEST · water exchange

Introduction

Molecular imaging aims at visualizing molecular events occurring in vivo at a cellular level. The possibility of repeatable, non-invasive assessment, characterization, and quantification of gene and protein function, protein–protein interactions, signal transduction, etc. makes molecular imaging particularly attractive in biomedical applications. Any molecular-imaging procedure requires an imaging probe that is specific for a given molecular event.[1] Owing to its exceptional spatial and temporal resolution, magnetic resonance imaging is one of the most-powerful state-of-the-art diagnostic modalities. The contrast of MR images is often enhanced by the use of paramagnetic agents, often Gd^{III} complexes, which allow a better delineation of morphology or function.[2] More recently, a fundamentally different contrast mechanism based on chemical-exchange saturation transfer has been proposed.[3] Paramagnetic chemical-exchange saturation transfer (PARACEST) agents, typically lanthanide complexes, contain paramagnetically shifted mobile protons in slow exchange with bulk water.[4] The irradiation of these protons affects the magnetic resonance signal of water protons through chemical exchange. PARACEST imaging offers the advantage of 1) turning the contrast on and off at will, 2) multiplex analysis by using more than one probe,

[a] Dr. T. Chauvin, Dr. É. Tóth
Centre de Biophysique Moléculaire, CNRS
rue Charles Sadron
45071 Orléans (France)
E-mail: eva.jakabtoth@cnrs-orleans.fr

[b] Dr. S. Torres, Dr. R. Rosseto, Dr. B. Badet, Dr. P. Durand
Centre de Recherches de Gif, ICSN-CNRS
Avenue de la terrasse
91198 Gif-surYvette Cedex (France)
E-mail: philippe.durand@icsn.cnrs-gif.fr

[c] Dr. J. Kotek
Department of Inorganic Chemistry
Universita Karlova v Praze
(Charles University in Prague)
Hlavova 2030, 12840 Prague 2 (Czech Republic)

Supporting information for this article is available on the WWW under http://dx.doi.org/10.1002/chem.201101779.

and 3) a relatively straightforward design of responsive reporters because all factors that influence the exchange will have an effect on the water signal. In recent years, much effort has been devoted to the development of Ln^{III} complexes that are capable of providing an MRI-detectable response to an in vivo stimulus. Among these, enzymatically activated agents have specific advantages. Molecular magnetic resonance imaging is often seen as being limited by the low (nanomolar) concentrations of the molecular targets. Enzymatic activity can be exploited to concentrate the imaging probe at the target site by converting an MRI-silent agent into an active one.

The detection of β-galactosidase (β-gal) is of particular interest in biological applications. The *lacZ* gene encoding β-galactosidase is a reporter routinely used to reveal genetic manipulations in molecular biology.[5] β-gal is used to detect gene expression on tissue sections, biopsies, and post-mortem samples using colorimetric substrates that are not suitable for long-term follow-up. NIR-fluorescent agents[6] or MRI-contrast agents[7] that are activated upon cleavage by β-gal and are applicable in non-invasive, live-animal imaging could be valuable tools to visualize changes in *lacZ* gene expression over time in deep tissues.[8] The first MRI agent to detect β-gal was reported by Meade and co-workers.[7] This galactopyranoside-capped Gd^{III} complex showed an increase in relaxivity upon exposure to β-gal, owing to increased water access to the Gd^{III} site. This probe has been used for the detection of the *lacZ* gene in *Xenopus laevis*. In another example, a Gd^{III} chelate bearing a 2-difluoromethylphenyl-β-galactopyranoside was used as a probe in which the β-galactosidase-catalyzed cleavage of the glycosidic bond induces formation of an electrophilic species that reacts covalently with human serum albumin (HSA) or β-galactosidase to yield macromolecular adducts and thus achieves a relaxivity change upon enzymatic activation (ca. 60% change in T_1). This probe was used to visualize β-gal expression in a mouse-tumor model.[9] Nagano and co-workers reported a β-gal-activated contrast agent based on the receptor-induced magnetization enhancement (RIME) phenomenon. A galactoside unit is linked to the Gd^{III} chelate through an albumin binding moiety that only becomes available for albumin interaction following enzymatic cleavage.[10] The compound exhibited an increase in relaxivity of 57% in phosphate-buffered saline (PBS, pH 7.4) with 4.5% w/v HSA in the presence of β-galactosidase.

Our approach to enzyme-responsive MRI-contrast agents is based on a "self-immolative" mechanism, where the action of a specific enzyme on the substrate moiety of the contrast agent initiates a self-immolation process. This "self-destructive" cascade reaction is expected to result in the transformation of the Ln^{III} complex with a concomitant change in the contrast-enhancement properties (Scheme 1). In the context of MRI, Meade and co-workers have reported a Gd^{III} complex containing a self-immolative linker, designed for detection of β-glucuronidase.[11] Self-immolative units are applied in antibody-directed enzyme prodrug therapy (ADEPT) or gene-directed enzyme prodrug therapy (GDEPT),[12] and are based on the intrinsic instability of benzylcarbamates that possess an electron-donor substituent at the *ortho* or *para* positions. Employing benzylcarbamates as self-immolative units allows the scope of the substrate to be any enzyme-recognized moiety that is capable of transitionally reducing the electron-donating properties of the substituent. This is a very general approach, which opens the way to the detection of a large variety of enzyme activities. Therefore, one can create enzyme-activated molecular-imaging probes that incorporate a MRI-reporting unit and a self-immolative chain onto the appropriate substrate to ensure enzyme specificity.

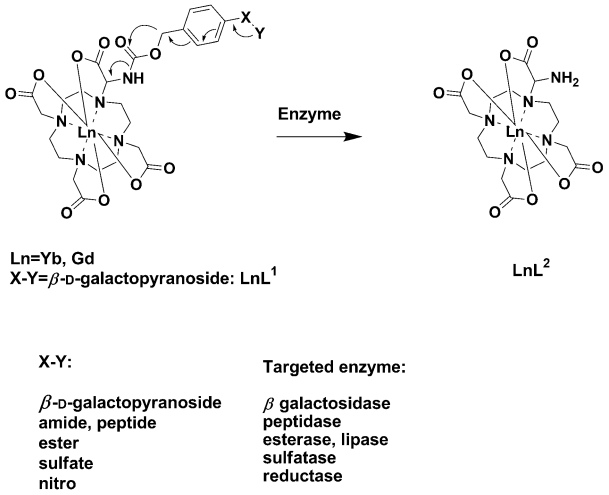

Scheme 1. Platform of self-immolative agents for the detection of enzyme activities.

We have recently reported the first example of an activatable contrast agent based on this versatile platform (**LnL^1**, Scheme 1).[13] Destruction of the self-immolative linker induced by enzyme cleavage was originally expected to afford an unstable,[14] 2-glycylsubstituted GdDO3A complex that would decompose into the bis-hydrated GdDO3A, thereby increasing the hydration number and thus the relaxivity. However, as established by HPLC/MS analysis of the enzymatic reaction mixture,[13] the self-immolative process led to the cleavage of the carbamate to yield the stable complex **GdL^2**, which was also observed during the course of a study by Yoo and Pagel (Scheme 1).[15] Indeed, literature examples confirmed that metal-coordination can stabilize *gem*-diamines.[16]

Ytterbium-complex **YbL^2** demonstrated a PARACEST effect. Exploiting this result, a prototype compound, Yb(dota-αbz-βGal)$^-$ (**YbL^1**, dota = 1,4,7,10-tetraazacyclododecane-*N*,*N*′,*N*″,*N*‴-tetraacetate) was designed to give a PARACEST response to the activity of β-galactosidase (Scheme 1).[13] In order to gain further insight into the peculiar behavior of these aminal derivatives, herein, we report the synthesis of various Gd^{III} and Yb^{III} complexes and their physicochemical characterization with potential applications as T_1 or PARACEST MRI probes (Scheme 2). We also

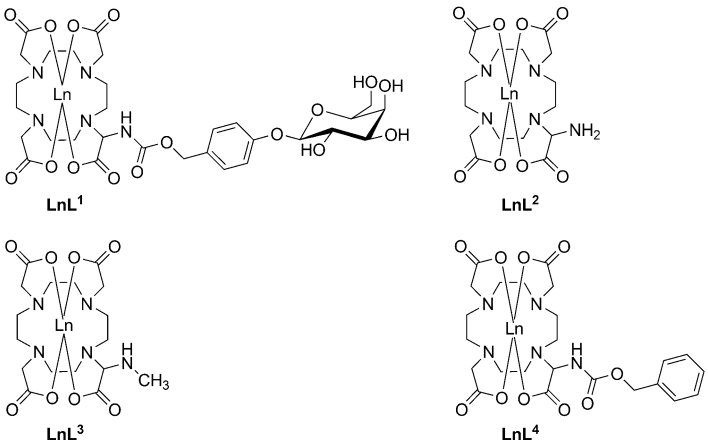

Scheme 2. Complexes studied in this work. (Ln = Gd, Yb).

extend the study to the *N*-methylated analogues as model compounds.

The starting Gd^{III} complex **GdL^1**, enzymatic-conversion product **GdL^2**, as well as two model compounds, **GdL^3** and **GdL^4**, were characterized with regard to their contrast-agent efficacy (Scheme 2). Variable-temperature ^{17}O NMR and ^1H NMRD measurements were performed to assess the parameters that influence their proton relaxivity. Luminescence lifetime and UV/Vis absorption measurements were performed on some Eu^{III} derivatives to quantify the bound water molecules and assess the hydration equilibria. The protonation states of the complexes bearing an exocyclic amine were determined by pH-potentiometric titrations. In addition, and to complete the work reported in our first communication,[13] we report the determination of proton-exchange rates of these Yb-derivatives as PARACEST probes.

Results and Discussion

Synthesis: We designed a synthetic pathway applicable to all of the targeted ligands (**L^1**–**L^4**) including the *O*-glycosylated derivative, **L^1** (Scheme 3). *N*-benzyloxycarbonyl α-aminoglycine intermediates (**3a**–**3d**) were obtained by amine addition to *N*-benzyloxycarbonyl imine (or iminium) acetates generated in-situ from activated α-heteroglycine precursors, such as α-acetoxy (**2a** and **2b**) or α-chloroglycines (**2c** and **2d**).[17] In this condensation reaction, we used the less-reactive ester derivative of *N*1,*N*4,*N*7-cyclentriacetic acid (DO3A)[18] rather than cyclen to avoid handling the poorly stable aminal intermediate. The commercially available triethyl ester of DO3A was preferred to the tri-*tert*-butyl ester because of the known instability of the glycosidic bond of **L^1** under acidic conditions, which are necessary for the ester deprotection. During the course of this work, the synthesis of complex **LnL^2** and its peptide derivatives was reported from the condensation of DO3A-*ter*-butyl ester with an α-bromoglycine derivative.[15] In our synthesis, each of the fully protected intermediates **3a**–**3d** could be isolated, but they all exhibited limited stability. Therefore, we preferred to synthesize complexes **LnL^1** and **LnL^4**–**LnL^6** from α-heteroglycines **2a**–**2d** without purification of the intermediates. Polymer-supported 1,5,7-triazabicyclo[4.4.0]dec-5-ene (TBD resin) was used as a base for the condensation reactions and the more-lipophilic 1-naphthylmethylcarbamate was substituted for the benzyl one in the case of complex **LnL^6** in order to facilitate the final purification of the lanthanide complexes.

The more-activated α-chloroglycines **2c** and **2d** were more suitable for the condensation of the N-methylated derivatives. In this case, triethylamine was used as the base but the intrinsic basicity of the DO3A ester was also sufficient to catalyze the reaction. The saponification and the subsequent complexation to the lanthanide were done in a classical way. Finally, the carbamate moiety of complexes **LnL^4**–**LnL^6** was removed by catalyzed hydrogenolysis using Pd/C

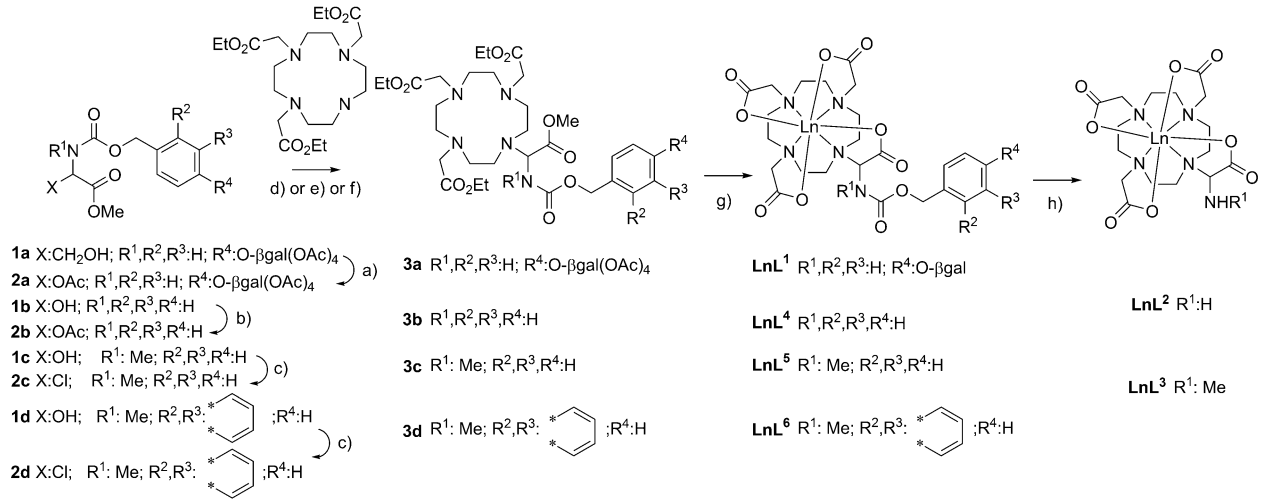

Scheme 3. Synthesis of **LnL^1**–**L^6**: a) see Ref. [13]; b) Ac_2O, Py, CH_2Cl_2, 0 °C; c) $SOCl_2$, CH_2Cl_2, reflux; d) **2b**, TBD resin, CH_2Cl_2, RT; e) **2c**, Et_3N, CH_2Cl_2, RT; f) **2d**, CH_2Cl_2, RT; g) i) NaOH, EtOH/H_2O 1:3 to 1:5, RT; ii) $LnCl_3{\cdot}xH_2O$, pH 6.5–7, RT; h) H_2O, Pd/C, H_2, RT. Py = pyridine.

under an atmosphere or a slight pressure of hydrogen to give the α-amino-glycine/dota complexes, **LnL²** and **LnL³**.

Characterization of the Gd^{III} complexes

Protonation constants of the GdL² and GdL³ complexes: The protonation constant of the non-coordinating exocyclic amine nitrogen atom has been determined by pH-potentiometric titrations for complexes **GdL²** and **GdL³** ([Eq. (1)], using equilibrium concentrations):

$$K_H = \frac{[GdLH]}{[GdL][H^+]} \quad (1)$$

The values obtained are $\log K_H = 5.12(\pm 0.01)$ and 5.99-(± 0.01) for complexes **GdL²** and **GdL³**, respectively. These protonation constants are about four orders of magnitude lower than those typically reported for primary or secondary amines. This result indicates that the exocyclic amino groups in both complexes are unprotonated at physiological pH, thus conferring a global negative charge on the complexes.[19] The surprisingly low basicity of the exocyclic amine nitrogen atoms in complexes **GdL²** and **GdL³** cannot only be rationalized by the presence of the *gem*-diamino motif or of the carboxylic-acid substituent because protonation constants of 7.8 and 8.9 have been reported for a mono-acetylated 1,1-diamine compound[20] and an α-amino-glycine derivative,[21] respectively. The coordination of the endocyclic nitrogen atom to the positively charged metal cation obviously contributes to the high acidity, as previously suggested for other *gem*-diamine-containing metal complexes.[16h] Indeed, a spectacular decrease of the protonation constant has been reported for the primary amine in Co^{2+} complexes formed with the α-diaminomalonate moiety($\log K_H = 1.6$)[16i] or for the tertiary amine in the Ni^{2+} complex formed with azacyclam ($\log K_H < 2$).[16h] In fact, coordination of the metal at such a short distance from the uncoordinated amine atom affords a strong electrostatic repulsion towards positively charged species, which makes the approach of the hydrogen ion difficult.[16h] Long-range interactions between the nitrogen atom and the electrons of the metal were also suggested to explain this effect.[16a] The crystal structures reported for α-diamine-containing metal complexes also revealed a very peculiar structural behavior: the C–N bond length for the coordinated nitrogen atom is longer than typical C–N single bonds, whilst that of the uncoordinated nitrogen atom is shorter than the typical length. In addition, the N-C-N bond angle is flatter than that of an sp^3 nitrogen atom. All of these results indicate a near-sp^2 hybridization of the uncoordinated amine nitrogen atom and a behavior that is more characteristic of aniline than of an aliphatic amine.[16a,b,d,f–l,22] One can also evoke the anomeric effect observed in systems containing X-C-Y motifs (X, Y=OR, NR_2, halogen),[23] the exact origin of which is still under debate[24] and which affects both structural and electronic properties. It has been established that an atom involved in an anomeric effect has a lower proton or cation affinity than a "normal" one.[25] Whilst the anomeric effect is negligible for neutral aminals, it is of higher magnitude for $R_2NCHRNR_3^+$ ions[23] and we suspect that it could be partly responsible for the low basicity of the exocyclic amine nitrogen atom of complexes **GdL²** and **GdL³**.

Moreover, according to the established mechanism for the hydrolysis of *gem*-diamine, the low basicity of the exocyclic amine atom could be also responsible for the unexpected stability of complex **LnL²** and **LnL³**, especially under acidic conditions.[20]

Determination of the number of coordinated water molecules: For all four Gd^{III} complexes, the coordination of a single inner-sphere water molecule is expected base on previous results for analogous lanthanide(III) complexes. This coordination was confirmed by luminescence-decay measurements on the Eu^{III} complexes of ligands L_1 and L_2. The luminescence lifetimes are $\tau_{H_2O} = 0.900$ ms, $\tau_{D_2O} = 2.740$ ms for complex **EuL¹** and $\tau_{H_2O} = 0.882$ ms, $\tau_{D_2O} = 2.565$ ms for complex **EuL²**. From these values and using well-established relationships,[26] we obtain $q = 0.8(\pm 0.3)$ for both complexes. The absence of hydration equilibria was confirmed by UV/Vis absorption spectra of aqueous solutions of complex **EuL¹** and **EuL²**. Both complexes exhibited one temperature-invariant absorption band in the 578–582 nm region, which corresponded to a $^5D_0 \leftarrow {}^7F_0$ transition (see the Supporting Information). This transition is very sensitive to the coordination environment and the observation of a single band excludes the co-existence of differently hydrated species.[27]

^{17}O NMR and ^1H NMRD measurements on the Gd^{III} complexes: The water-exchange rate was determined for the Gd^{III} complexes of ligands **L¹**, **L²**, **L³**, and **L⁴** from a variable-temperature ^{17}O NMR study. In order to assess the effect of the protonation of the amine on the water-exchange parameter of complex **GdL²**, measurements at two different pH values (pH 4.6 and 6.6) were performed, which correspond to conditions in which the amine is mainly in its protonated and unprotonated forms, respectively ($\log K_H = 5.12$). Owing to the instability of the complex below pH 4, a further decrease in pH value to attain a fully protonated amine form was not possible. In addition, variable-temperature proton-relaxation rates (25 and 37 °C) were measured for complexes **GdL¹**, **GdL²**, and **GdL⁴** as a function of the proton Larmor frequency (NMRD profiles), with the objective of determining parameters that describe rotation. The ^{17}O NMR chemical shifts ($\Delta\omega_r$), transverse relaxation rates ($1/T_{2r}$), and the proton relaxivities (r_1) were analyzed simultaneously using the Solomon–Bloembergen–Morgan (SBM) theory of paramagnetic relaxation (see the Supporting Information). If we are not interested in detailed information about the electron-spin relaxation and if we restrict the analysis of the NMRD data to medium- and high magnetic fields, this SBM approach gives reliable information on dynamic processes like water-exchange and rotational correlation times for small complexes.[28] Therefore, we included only relaxivity values above 6 MHz in the simultaneous fit

and the following parameters have been adjusted: the water-exchange rate (k_{ex}^{298}), the activation enthalpy for water exchange ($\Delta H^{\neq}$), the scalar coupling constant ($A/\hbar$), the rotational correlation time (τ_R^{298}) and its activation energy (E_R), and the parameters describing electron-spin relaxation, the mean square of the zero-field splitting (Δ^2), the correlation time for the modulation of the zero-field splitting (τ_V^{298}), whilst its activation energy (E_V) has been fixed to 1 kJ mol^{-1}. The scalar coupling constants obtained in this way are in the usual range for Gd^{III} complexes; this observation justifies the assumption of $q=1$. The experimental ^{17}O NMR and NMRD data and the fitted curves for **GdL^1** are presented in Figure 1, the data and curves for the other complexes are shown in the Supporting Information.

The shape of the NMRD curves and their temperature dependence (r_1 decreases with increasing temperature) follows the general trend observed for typical small-molecular-weight complexes. At low temperatures, and for all Gd^{III} complexes studied, the transverse ^{17}O relaxation rates ($1/T_{2r}$) increase with increasing temperature, thereby indicating that these systems are in slow exchange, as expected for dota-analogue complexes. Here, $1/T_{2r}$ is directly determined by the water-residence time ($\tau_m=1/k_{ex}$). At higher temperatures, the systems turn to a fast-exchange regime, where the transverse ^{17}O-relaxation rates are also influenced by the longitudinal electronic-relaxation rate ($1/T_{1e}$) and the nuclear hyperfine coupling constant ($A/\hbar$). All parameters obtained in the fit are shown in Table 1.

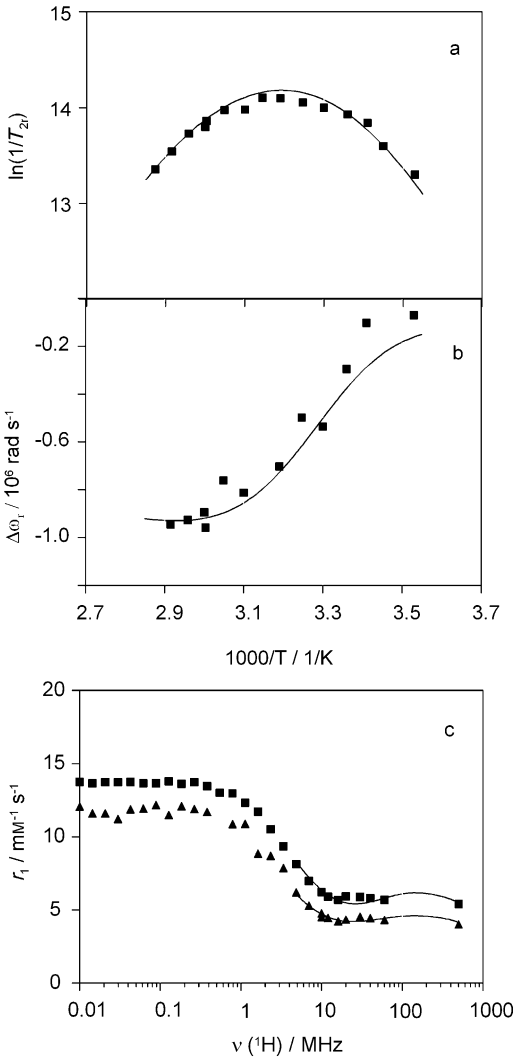

Figure 1. Temperature dependence of a) the reduced transverse ^{17}O relaxation rates ($1/T_{2r}$), and b) ^{17}O chemical shifts ($\Delta\omega_r$) for **GdL^1**. c) Proton relaxivities (r_1) as a function of the Larmor frequency at 25 °C (ν) and 37 °C (▲). The lines represent the best fits to the experimental points. For **GdL^2–GdL^4**, see the Supporting Information.

Water exchange and rotation: The exchange rates for all four systems are slightly lower than that of [Gd(dota)] (Table 1), with small differences from one complex to the other. The mechanism remains dissociatively activated, as shown by the positive activation entropies. In general terms, the rate and mechanism of the water-exchange rates are closely related to the inner-sphere solution structures of the complexes. The water-exchange rate is little affected by substituents that do not directly interfere in the inner coordination sphere. The destruction of the self-immolative arm does not lead to a significant change in the water-exchange process: complexes **GdL^1** and **GdL^2** exhibit similar water-exchange rates despite the removal of one pending arm. It is also known that in dissociatively activated water-exchange processes, the charge of the complex is important: a higher overall negative charge favors the release of the water molecule, thus accelerating the exchange. We observe the same trend in the k_{ex}^{298} value determined for complex **GdL^2** at the two different pH values: at pH 6.6, the complex is not protonated at the exocyclic amine atom, and therefore its overall charge is −1 whilst at pH 4.6 it

Table 1. Kinetic and structural parameters obtained for complexes [**GdL$^{1-4}$(H$_2$O)**] from the fitting of ^{17}O NMR and NMRD data. Values in italic type were fixed in the fitting procedure.

Ligand	**L^1**[a]	**L^2**[a,c]	**L^3**[b]	**L^4**[a]	**DOTA^{4-}**[a,d]
$k_{ex}^{298}\times10^{-6}$ [s^{-1}]	2.5(±0.5)	3.9(±0.2) 1.5(±0.5)	1.9(±0.2)	2.2(±0.4)	4.1(±0.2)
$\Delta H^{\neq}$ [kJ mol^{-1}]	59.0(±1.0)	46.0(±1.0) 39.7(±1.2)	55.2(±1.8)	51.6(±1.6)	49.8(±1.5)
$\Delta S^{\neq}$ [J mol^{-1} K]	92(±5)	25(±4) 7(±6)	36.3(±3.7)	16.6(±3.1)	48.5(±4.9)
τ_{RH}^{298} [ps]	130(±10)	85(±7)	–	110(±10)	77(±4)
E_R [kJ mol^{-1}]	23.0(±1.8)	25.0(±2.1)	–	21.4(±2.0)	16.1(±7.4)
$A/\hbar\times10^{-6}$ [Hz]	−3.6(±0.3)	−3.8(±0.3) −3.8(±0.3)	−3.8(±0.3)	−3.6(±0.3)	−3.7(±0.2)

[a] determined by ^{17}O NMR and NMRD spectroscopy. [b] From ^{17}O NMR spectroscopic relaxation rates and chemical shifts. [c] Values determined at pH 6.6 (top line) and 4.5 (bottom line), respectively; at pH 4.5 only from ^{17}O NMR data. [d] From Ref. [29]

is protonated and becomes neutral. Consequently, the water-exchange rate of complex **GdL²** is reduced by a factor of approximately 2 between pH 6.6 and 4.6.

The rotational correlation times calculated for these Gd^{III} complexes are reasonable for the size of the molecule and their trend reflects their increasing size from **GdL²** to **GdL⁴** and **GdL¹**.

Variation in relaxivity upon enzymatic cleavage: Contrary to our original expectations, the cleavage of **GdL¹** and the subsequent self-immolative reaction does not proceed until the formation of the GdDO3A complex, which would result in an increase in the hydration number from $q=1$ to 2. Therefore, the variation in relaxivity upon enzymatic cleavage is only caused by a decrease in the complex size, that is, the rotational correlation time, and it amounts to between 10–20%, depending on the temperature and the proton Larmor frequency (Table 2). Such a small change in relaxivity is likely insufficient for the in vivo detection of enzymatic activities using these complexes. However, one can imagine that the cleavage of larger macromolecular probes of complexes **GdL²** or **GdL³** attached to a dendrimeric structure through self-immolative linkers would result in considerable diminution of the rotational correlation time, and thus of the relaxivity.

Table 2. Relaxivity of the Gd^{III} complexes before (**GdL¹**) and after enzymatic cleavage (**GdL²**).

r_1 [$mM^{-1}s^{-1}$]	20 MHz		60 MHz	
	25 °C	37 °C	25 °C	37 °C
GdL¹	5.57	3.72	4.83	3.68
GdL²	4.38[a]	3.38	4.11	3.15

[a] $r_1=4.83$ $mM^{-1}s^{-1}$ was reported for **GdL²** at 600 MHz.[15]

Characterization of the Yb^{III} complexes: In a previous communication on the Yb^{III} complexes of **L¹** and **L²**,[13] we reported that no PARACEST effect is detectable for complex **YbL¹**, despite the presence of a carbamate proton, in contrast to the PARACEST effect found for the Tm^{III} complex of related derivatives.[30] After incubation with β-galactosidase, a PARACEST effect is observed at $\delta=-16.7$ and $\delta=-20.5$ ppm, owing to the two slowly exchanging, magnetically non-equivalent amine protons. A PARACEST effect was also reported for the **TmL²** complex at $\delta=+8$ ppm, but this effect was difficult to exploit.[30] Here, our objective was to complete the preliminary study of the substrate and the product of the enzymatic reaction with respect to their PARACEST behavior, in particular to determine their proton-exchange rate. In order to assess the effect of amine substitution on the PARACEST properties, we also investigated the methyl-amine derivative **YbL³**. As expected, a single CEST peak was detected for the secondary amine of **YbL³** at $\delta\approx-25$ ppm, in the same region as for complex **YbL²**. The CEST effect exhibits a strong pH-dependency (Figure 2). High-resolution NMR spectroscopic analysis showed a broad peak corresponding to the CEST effect of the amine proton ($\delta=-26$ ppm; Figure 3). This signal broadens with decreasing pH value and disappears below pH 8, thereby indicating an increasingly fast proton exchange when the pH value is decreased. The fact that the secondary amine group is also capable of providing a CEST effect opens up the possibility of functionalizing this amine group to link the PARACEST probe to biomacromolecules, or to form macromolecular structures.

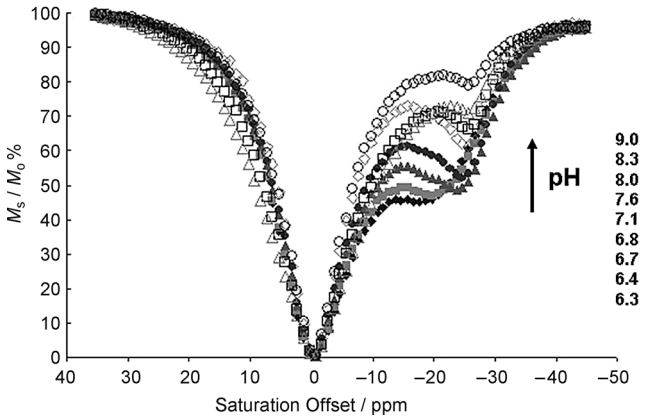

Figure 2. CEST spectra recorded for **YbL³** (37 °C, [**YbL³**] = 20 mM) at various pH values.

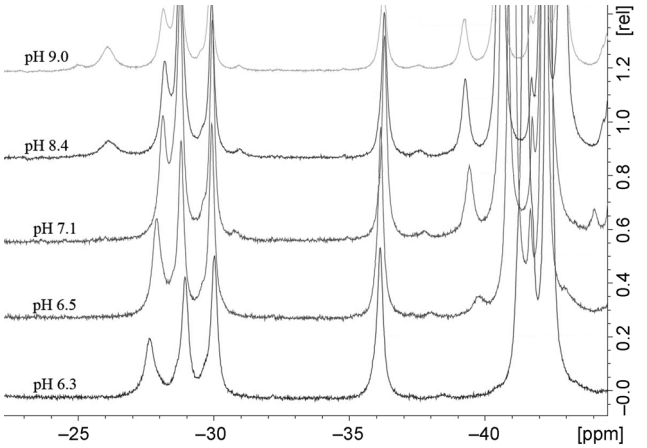

Figure 3. 500 MHz ^1H NMR spectra of a 20 mM aqueous solution of **YbL³** at various pH values (37 °C, $\delta_{bulk\,water}=0$ ppm).

Determination of the proton-exchange rates: To explain the evolution of the CEST effect for complexes **YbL²** and **YbL³**, we determined the exchange rate of the mobile protons on both complexes at various pH values. Several methods are available to estimate the proton-exchange rate from the CEST effect. One of them uses the concentration dependence of the saturation transfer, as shown in Equation (2):[31]

$$\left(\frac{M_s}{M_0}\right)=\frac{1}{1+\frac{k_{ex}[C]nT_1}{111}} \qquad (2)$$

where M_s is the signal intensity of the bulk water protons taken immediately after the pulse is applied to the exchangeable protons of the CEST agent, M_0 is the initial intensity of bulk water protons in the absence of saturation, k_{ex} is the exchange-rate constant, n is the number of saturated protons per CEST molecule, $[C]$ is the concentration of the CEST agent, and T_1 is the longitudinal relaxation time of bulk water protons.

One can also determine the proton-exchange rate from the saturation time and saturation-power dependency of the intensity of the water proton (QUEST and QUESP experiments refer to quantification of the exchange rate as a function of saturation time or saturation power, respectively).[32] Assuming that the steady state is reached upon saturation of the solute, Equation (3) applies,[32] where x_{CA} is the fractional concentration of exchangeable protons of the contrast agent, t_{sat} is the saturation time, α is the saturation efficiency, and k_{ex} is the rate of proton exchange on the amine:

$$1-\frac{M_s}{M_0}=\frac{k_{ex}\alpha x_{CA}}{R_{1W}+k_{ex}x_{CA}}\times\left[1-e^{-(R_{1W}+k_{ex}x_{CA})t_{sat}}\right] \quad (3)$$

The saturation efficiency depends on the pulse power, [Eq. (4)], where $R_{1,2S}$ and $R_{1,2W}$ are the longitudinal- and transverse relaxation rates of the solute and the bulk water in the saturated state, respectively:

$$\alpha=\frac{\omega_1^2}{\omega_1^2+pq} \quad (4)$$

$$p=R_{2S}+k_{ex}-\frac{k_{ex}^2x_{CA}}{R_{2W}+k_{ex}x_{CA}} \quad (5)$$

$$q=R_{1S}+k_{ex}-\frac{k_{ex}^2x_{CA}}{R_{1W}+k_{ex}x_{CA}} \quad (6)$$

The values of $1-M_s/M_0$ obtained as a function of saturation time are often analyzed according to Equation (7), as reported by Zhang et al,[33] where both k_{ex} and the longitudinal relaxation time, T_1, are used to make the fit:

$$1-\frac{M_S}{M_0}=1-\left(\frac{1}{1+k_{ex}x_{CA}T_1}+\frac{k_{ex}x_{CA}T_1}{1+k_{ex}x_{CA}T_1}e^{-(1+k_{ex}x_{CA}T_1)t_{sat}}\right) \quad (7)$$

Each of these techniques requires that the agent concentration is known. Recently, Dixon et al. have reported a modified analysis of the QUESP experiment as a concentration-independent method to assess the proton-exchange rate in PARACEST agents.[34] They derived Equation (8), where ω_1 is the amplitude of the radiofrequency applied for the saturation pulse given in rad s^{-1}:

$$\frac{M_S}{M_0-M_S}=\frac{55.5}{c}k_{ex}R_{1w}\left(\frac{1}{k_{ex}^2}+\frac{1}{\omega_1^2}\right) \quad (8)$$

A plot of $M_s/(M_0\text{-}M_S)$ versus $1/{\omega_1}^2$ (referred to as an omega plot) should be linear with an x-axis intercept ($M_s/(M_0-M_s)=0$) to providing the exchange rate directly, $-1/{k_{ex}}^2$ [Eq. (9)]:

$$-\frac{1}{k_{ex}^2}=\frac{1}{\omega_1^2} \quad (9)$$

The derivation of this linear relationship assumes that k_{ex} is much higher than the longitudinal- and transverse relaxation rates.

We have used these various methods to assess the exchange rate on the complexes **YbL²** and **YbL³**. Variation of the concentration and QUEST measurements were performed on complex **YbL²**, whilst the exchange rate of **YbL³** was determined from: 1) a simultaneous analysis of QUEST and QUESP data, 2) a fit of the saturation-time-dependent data to Equation (7), and 3) a fit of the QUESP data to Equation (8). First, we will discuss the data for complex **YbL³**, because, for this system in particular, we assessed the value of QUESP measurements in calculating proton-exchange rates. Proton-exchange rates reported in the literature are typically determined from saturation-time-dependent experiments, and we wanted to assess whether the saturation-power-dependency experiments make the determination more accurate in combination with QUEST data, as previously suggested for diamagnetic systems,[32] and whether the concentration-independent approach of the QUESP analysis is applicable.

Figure 4 shows the dependence of the CEST effect of complex **YbL³** on saturation time and saturation power at

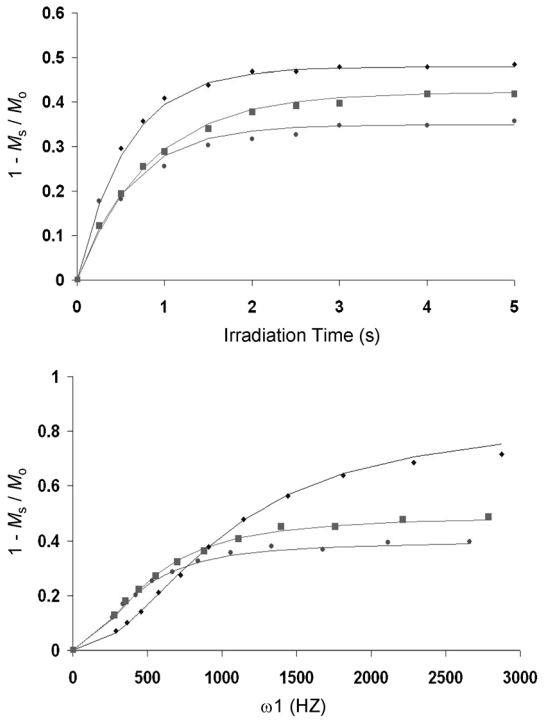

Figure 4. QUEST (top) and QUESP (bottom) data for **YbL³**. The curves represent a simultaneous fit to Equations (3)–(6).

different pH values, measured at $\delta = -26$ ppm. All of the QUEST and QUESP data have been fitted simultaneously to Equations (3)–(6) to obtain the rate of proton exchange. The fitted values of R_{1W} and R_{2W} were in the range 0.4–0.5-($\pm$0.2) s^{-1} and their variation were within $\pm$50%; as such, these results led to no significant alteration of the calculated proton-exchange rate. R_{1S} is negligible compared to k_{ex} and has no influence on the fit. The transverse relaxation rate of the solute R_{2S} has been calculated in the fit to give 130-($\pm$40) s^{-1} at any pH value. We should note that the k_{ex} values remained unaffected even by a relatively large (several fold) variation of R_{2S}. The QUEST experiments were also fitted to Equation (7) (see the Supporting Information). The QUESP data were also analyzed according to Equation (8) (for pH 8.4, see Figure 5; data for the other pH values are

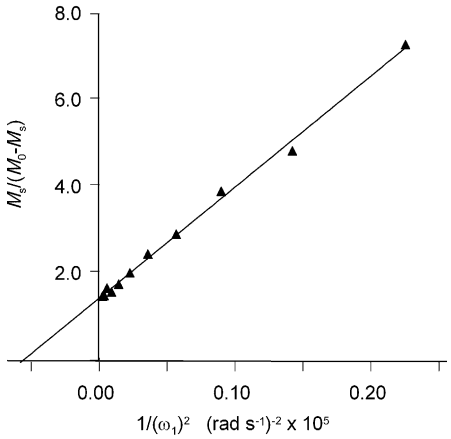

Figure 5. Omega plot for **YbL³** at pH 8.4. The curve represents the fit to Equation (8).

shown in the Supporting Information). They indeed fall on a straight line, as shown for the $[Eu(DOTA)(glyOEt)_4]^{3+}$ system.[34] The best-fit values are listed in Table 3.

Table 3. k_{ex} [s^{-1}] values obtained for **YbL³** at 310 K.

	pH value			
	6.4	6.9	7.4	8.4
QUEST + QUESP	5500($\pm$500)	3800($\pm$500)	1500($\pm$500)	1200($\pm$500)
QUEST [Eq. (7)]	2900($\pm$800)	3200($\pm$800)	1800($\pm$500)	1500($\pm$500)
"omega plot"	6000($\pm$800)	4300($\pm$600)	1600($\pm$500)	1300($\pm$500)
x_{CA}[a]	0.288×10^{-3}	0.285×10^{-3}	0.286×10^{-3}	0.287×10^{-3}

[a] Fixed in the fit.

Very similar proton exchange rates were obtained from the different approaches (Table 3) for a given pH value. The method based on the omega plot was previously validated for a Eu^{3+} complex in which the CEST effect originated from the slow exchange of the coordinated water molecules.[34] For our **YbL³** complex, the proton exchange is around ten times faster than in $[Eu(DOTA)(glyOEt)_4]^{3+}$, which is important with respect to the condition of k_{ex} being considerably higher than the relaxation rates. This simple analysis of the QUESP data, when applicable, provides a very convenient way of determining the k_{ex} value, because this method avoids the concentration effect and also does not include the fitting of the longitudinal- and transverse relaxation rates, which are not directly accessible by independent measurements.

For complex **YbL²**, the rate constants of the exchangeable NH_2 protons ($\delta = -23$ ppm and $\delta = -16$ ppm) were either estimated from: 1) a concentration-dependent study of the saturation transfer in the range of 1–75 mM (pH 7.4; Figure 6) by fitting the results to Equation (2) (Table 4), or

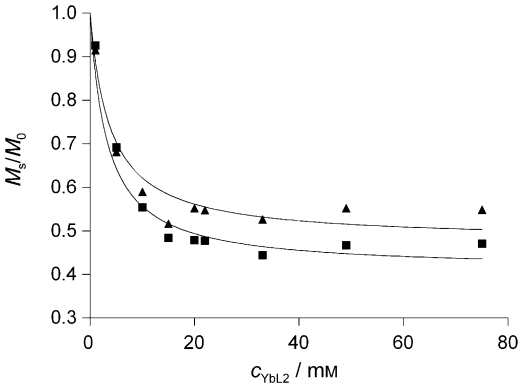

Figure 6. Concentration dependence of the CEST effect for **YbL²** at $\delta = -16$ ppm (ν) and $\delta = -23$ ppm (π). The curve represents the fit to Equation (2).

Table 4. k_{ex} values obtained from the best fit of QUEST data of **YbL²** to Equation (7) at 310 K.

pH	k_{ex} [s^{-1}]		T_{1sat} [s]	
	$\delta = -16$ [ppm]	$\delta = -23$ [ppm]	$\delta = -16$ [ppm]	$\delta = -23$ [ppm]
6.4	–	3500($\pm$500)	–	1.4($\pm$0.1)
6.9	2000($\pm$500)	2800($\pm$500)	1.1($\pm$0.1)	1.1($\pm$0.1)
7.4	1600($\pm$500)	2100($\pm$500)	1.2($\pm$0.1)	1.3($\pm$0.1)
	1700($\pm$500) [a]	2200($\pm$500)[a]		
8.0	1000($\pm$500)	1700($\pm$500)	1.1($\pm$0.1)	1.1($\pm$0.1)

[a] From concentration-dependent measurements.

from 2) the dependence of the CEST effect on the saturation time (see the Supporting Information). These results indicate that the CEST effect does not increase when the saturation time is increased beyond 2 s. From the measurements, we were able to distinguish the two amine protons. We fitted the QUEST experiments performed at different pH values to Equation (7) and the k_{ex} values obtained with this method are reported in Table 4.

The exchange rates of the amine protons obtained for complexes **YbL²** and **YbL³** are of the order 10^3 s^{-1}, similar to those reported in the literature for amide protons of Yb^{3+}-DOTAM complexes (DOTAM = 1,4,7,10-tetrakis(carbamoylmethyl)-1,4,7,10-tetrazacyclododecane), which are well-known to give rise to an observable CEST effect. For complex **YbL²**, the proton at $\delta = -16$ ppm exchanges slightly

more slowly than the proton at $\delta = -23$ ppm. A similar difference in the exchange rate has been previously reported for the two magnetically non-equivalent NH_2 protons of the Yb^{3+}-DOTAM complex.[35] To the best of our knowledge, no proton-exchange rates have been reported for amine groups in metal complexes. The exchange rate of the amine function of acetyl-lysine-NH_2 was $4000\ s^{-1}$, whilst exchange rates for arginine of $700\ s^{-1}$ and $1200\ s^{-1}$ correspond to the εNH and ηNH_2 groups, respectively.[36,37] For the amine protons of both complexes **YbL²** and **YbL³**, we observe a systematic decrease of the exchange rate with increasing pH value, which is also translated by a diminution of the observed CEST effect. This trend is similar to that observed for aniline protons[37] and for the amine of the **TmL²** complex.[38]

However this trend is opposite to the typical behavior of the amide protons in Ln^{3+}-DOTAM complexes, for which the proton exchange is a base-catalyzed process, with a concomitant increase of the CEST effect with increasing basicity.[39] For instance, the CEST effect measured in a 30 mM solution of the tetraglycinate-derivative Yb-DOTAM-Gly changes from 0 to about 65% between pH 5.5 and 8.0,[39] whilst for complex **YbL³**, it decreases from 65% at pH 6.3 to 15% at pH 9.0. The aniline-like behavior of the amine groups of complexes **YbL²** and **YbL³** could be explained by their near-sp^2 hybridization caused by lanthanide coordination of the *gem*-diamine, moiety as previously discussed. For the proton exchange of amines, both acid- and base-catalysis has been reported.[36] It is interesting to note that a plot of log k_{ex} values versus the pH value for both complexes (and for both protons of **YbL²**) gives a straight line, in accordance with the general formula of acid catalysis ($k_{ex} = k_0 + k_H[H^+]$; also see the Supporting Information).

Conclusions

We have designed and synthesized DOTA derivatives of α-aminoglycine and their corresponding lanthanide complexes as building blocks for self-immolative imaging probes. A synthetic pathway giving access to the platform with or without the self-immolative linker and without the difficulties associated with the intrinsic instability of these ligands was elaborated. The physicochemical properties of several Gd^{3+} complexes were investigated: a chelate bearing a self-immolative arm and a sugar unit as a selective substrate for β-galactosidase, its enzymatic product, and two model compounds. They all have one inner-sphere water molecule and consequently only slightly different proton relaxivities. This similarity precludes the application of the **GdL¹** complex as enzyme-specific T_1 relaxation agents. The water exchange for all four systems is slightly slower than for GdDOTA. The complexes containing exocyclic NH_2 or $NH(CH_3)$ amine groups are not protonated at physiological pH, as evidenced by pH-potentiometric measurements. Their Yb^{3+} analogues show a pH-dependent PARACEST effect. The proton-exchange rate was determined for both complexes at various pH values by using the dependency of the CEST effect on concentration, saturation time, and saturation power. We also applied a concentration-independent analysis of the saturation power dependency data, as recently proposed by Sherry and co-workers.[33] These different methods gave similar results. In contrast to the typically base-catalyzed amide-proton exchange on [Ln(dota)]/tetraamide complexes, the exchange of the amine protons becomes faster upon decreasing the pH value, which then leads to an increasing CEST effect at lower pH values.

Experimental Section

NMR measurements: ^1H and ^{13}C NMR spectra were recorded at 300 MHz and 75 MHz, respectively, and calibrated using tetramethylsilane as an internal reference. Variable-temperature ^{17}O NMR measurements of aqueous solutions of the Gd^{III} complexes were obtained on a Bruker Avance 500 spectrometer (11.75 T, 67.8 MHz) and referenced to an acidified water solution (aqueous $HClO_4$, pH 4). Longitudinal ^{17}O NMR relaxation times (T_1) were measured by the inversion-recovery pulse sequence,[40] and the transverse relaxation times (T_2) were obtained by the Carr–Purcell–Meiboom–Gill spin-echo technique.[41] To eliminate susceptibility corrections to the chemical shifts, the samples were sealed in glass spheres that fitted into 10 mm NMR tubes.[42] To improve sensitivity in the ^{17}O NMR spectra, ^{17}O-enriched water (10% $H_2{}^{17}O$, Cortecnet) was added to the solutions to yield 1% ^{17}O enrichment. The temperature was calculated according to a previous calibration with ethylene glycol and methanol.[43] The concentrations and pH values of the samples were: [**GdL¹**] = 14.2 mmol kg^{-1}, pH 7.10; [**GdL²**] = 13.7 mmol kg^{-1}, pH 4.50; [**GdL²**] = 10.3 mmol kg^{-1}, pH 6.60; [**GdL³**] = 24.7 mmol kg^{-1}, pH 6.90; [**GdL⁴**] = 12.6 mmol kg^{-1}, pH 7.20. The pH values of the solutions were adjusted by using diluted solutions of NaOH and HCl. The saturation-transfer experiments were performed on a Bruker Avance 500 spectrometer by irradiating the sample at 0.1 ppm increments. CEST spectra were recorded using pre-saturation pulses of 3 s duration at 25 μT, unless otherwise stated. Spectra were measured by recording the signal intensity of the bulk water as a function of the presaturation frequency. For QUEST experiments (quantification of the *e*xchange rate as a function of *s*aturation time), data were collected by varying the saturation time (0.25, 0.5, 1, 1.5, 2, 2.5, 3, 4, 5 s) at constant power (25 μT). The QUESP data (quantification of the exchange rate as a function of *s*aturation power) were collected by varying the saturation power whilst the saturation time remained constant (3 s). The QUEST and QUESP data were fitted with Scientist (MicroMath, Inc.).

NMRD measurements: The $1/T_1$ nuclear magnetic relaxation dispersion (NMRD) profiles of the Gd^{III} complexes were recorded on a Stelar SMARtracer FFC fast-field-cycling relaxometer covering magnetic fields from 2.35×10^{-4} T to 0.25 T, which corresponded to a proton Larmor frequency range of 0.01–10 MHz. The relaxivity at higher fields was recorded using a Bruker WP80 adapted to variable field measurements and controlled by the SMARtracer PC NMR console. The temperature was controlled by a VTC90 temperature-control unit and fixed by a gas flow. The temperature was determined according to a previous calibration with a platinum resistance temperature probe. The relaxivity at 500 MHz was measured on a Bruker Avance 500 (11.75 T) spectrometer. The simultaneous-least-squares fit of the ^{17}O NMR and ^1H NMRD data were performed by using Micromath Scientist version 2.0 (Salt Lake City, UT, USA). The reported errors correspond to one standard deviation obtained by statistical analysis.

UV/Vis spectrophotometry: Absorbance spectra were recorded on a Perkin–Elmer Lambda 19 spectrometer in thermostated cells between 25 and 50 °C for **EuL¹** ($c_{Eu} \approx 2.5$ mM, pH ≈ 6.80) and **EuL²** ($c_{Eu} \approx 2.4$ mM, pH ≈ 6.90). The measurements were carried out in a cylindrical cuvette with 10 cm optical path-length between $\lambda = 577$–581.0 nm.

Luminescence: The luminescence measurements of Eu^{III} complexes were performed on a Luminescence Thermo Spectronic spectrometer AMINCO Bowman Series 2. The luminescence spectra were obtained after excitation at the Eu^{III} $^5L_6 \leftarrow {}^7F_0$ band ($\lambda = 396$ nm). All measurement were performed at room temperature.

pH potentiometry: Protonation constants of the **GdL²** and **GdL³** complexes were determined by pH-potentiometric titration at 25 °C in 0.1 M KCl. The samples (3 mL) were stirred whilst a constant flow of N_2 was bubbled through the solutions. Titrations of about 3 mM **GdL²** and **GdL³** solutions (starting pH ≈ 4.5) were carried out by adding standardized KOH solution with a Metrohm 702 SM Titrino automatic burette. A Metrohm 692 pH/ion-meter was used to measure the pH value. The concentration of H^+ ions was determined from the measured pH values using the correction method proposed by Irving et al.[44] The protonation and stability constants were calculated from parallel titrations with the PSEQUAD program.[45] The errors given correspond to a single standard deviation.

Acknowledgements

This work was financially supported by the Centre National de la Recherche Scientifique, the Interdisciplinary program "Imagerie du Petit Animal" (CNRS), the European network (EMIL) No. 50356, and the ANR (ENZYMRI and ENZYMAGE). This work was performed within the European COST Action D38 "Metal-Based Systems for Molecular Imaging Applications". Financial support from the Grant Agency of the Czech Republic for J.K. (No. P207/11/1437), from the Institute of Chemistry of Natural Susbtances (ICSN) for S.T., and from the CNRS for R.R. is greatly acknowledged.

[1] *Acc. Chem. Res.* **2009**, *42*, issue 7, special issue on molecular imaging.
[2] A. E. Merbach, É. Tóth, *The Chemistry of Contrast Agents in Medical Magnetic Resonance Imaging*, Wiley, New York, **2001**, p. 471.
[3] K. M. Ward, A. H. Aletras, R. S. Balaban, *J. Magn. Reson.* **2000**, *143*, 79–87.
[4] S. Viswanathan, Z. Kovacs, K. N. Green, S. J. Ratnakar, A. D. Sherry, *Chem. Rev.* **2010**, *110*, 2960–3018.
[5] C. M. Watson, P. A. Trainor, T. Radziewic, G. J. Pelka, S. X. Zhou, M. Parameswaran, G. A. Quinlan, M. Gordon, K. Sturm, P. P. L. Tam, *Methods Mol. Biol.* **2008**, *461*, 149–164.
[6] a) C.-H. Tung, Q. Zeng, K. Shah, D.-E. Kim, D. Schellingerhout, R. Weissleder, *Cancer Res.* **2004**, *64*, 1579–1583; b) V. Josserand, I. Texier-Nogues, P. Huber, M. Favrot, J. L. Coll, *Gene. Ther.* **2007**, *14*, 1587–1593; c) G.-J. Zhang, T.-B. Chen, B. Connolly, S.-A. Lin, R. Hargreaves, A. Vanko, B. Bednar, D. J. MacNeil, C. Sur, D. L. Williams, *Assay Drug Dev. Technol.* **2009**, *7*, 391–399.
[7] a) M. M. Alauddin, A. Y. Louie, A. Shahinian, T. J. Meade, P. S. Conti, *J. Nucl. Med.* **2002**, *43*, 138P–139P; b) R. A. Moats, S. E. Fraser, T. J. Meade, *Angew. Chem.* **1997**, *109*, 749–752; *Angew. Chem. Int. Ed. Engl.* **1997**, *36*, 726–728; c) L. M. Urbanczyk-Pearson, F. J. Femia, J. Smith, G. Parigi, J. A. Duimstra, A. L. Eckermann, C. Luchinat, T. J. Meade, *Inorg. Chem.* **2008**, *47*, 56–68; d) L. M. Urbanczyk-Pearson, T. J. Meade, *Nat. Protoc.* **2008**, *3*, 341–350; e) M. M. Alauddin, A. Y. Louie, A. Shahinian, T. J. Meade, *Nucl. Med. Biol.* **2003**, *30*, 261–265.
[8] J. H. Kang, J.-K. Chung, *J. Nucl. Med.* **2008**, *49*, 164S–179S.
[9] Y.-T. Chang, C.-M. Cheng, Y.-Z. Su, W.-T. Lee, J.-S. Hsu, G.-C. Liu, T.-L. Cheng, Y.-M. Wang, *Bioconjugate Chem.* **2007**, *18*, 1716–1727.
[10] K. Hanaoka, K. Kikuchi, T. Terai, T. Komatsu, T. Nagano, *Chem. Eur. J.* **2008**, *14*, 987–995.
[11] J. A. Duimstra, F. J. Femia, T. J. Meade, *J. Am. Chem. Soc.* **2005**, *127*, 12847–12855.
[12] a) P. L. Carl, P. K. Chakravarty, J. A. Katzenellenbogen, *J. Med. Chem.* **1981**, *24*, 479–480; b) J.-L. Guerquin-Kern, A. Volk, E. Chenu, R. Lougerstay-Madec, C. Monneret, J.-C. Florent, D. Carrez, A. Croisy, *NMR Biomed.* **2000**, *13*, 306–310; c) R. Madec-Lougerstay, J.-C. Florent, C. Monneret, *J. Chem. Soc. Perkin Trans. 1* **1999**, 1369–1375; d) F. M. H. de Groot, W. J. Loos, R. Koekkoek, L. W. A. vanBerkom, G. F. Busscher, A. E. Seelen, C. Albrecht, P. deBruijn, H. W. Scheeren, *J. Org. Chem.* **2001**, *66*, 8815–8830.
[13] T. Chauvin, P. Durand, M. Bernier, H. Meudal, B.-T. Doan, F. Noury, B. Badet, J.-C. Beloeil, É. Tóth, *Angew. Chem.* **2008**, *120*, 4442–4444; *Angew. Chem. Int. Ed.* **2008**, *47*, 4370–4372.
[14] J. M. Z. Gladych, D. Hartley in *Comprehensive Organic Chemistry: the synthesis and reactions of organic compounds, Vol. 2* (Eds.: D. Barton, W. D. Ollis), Pergamon Press, New York, **1979**, pp. 61–130.
[15] B. Yoo, M. D. Pagel, *Tetrahedron Lett.* **2006**, *47*, 7327–7330.
[16] a) I. I. Creaser, R. J. Geue, J. M. Harrowfield, A. J. Herlt, A. M. Sargeson, M. R. Snow, J. Springborg, *J. Am. Chem. Soc.* **1982**, *104*, 6016–6025; b) M. P. Suh, W. Shin, D. Kim, S. Kim, *Inorg. Chem.* **1984**, *23*, 618–620; c) M. P. Suh, D. Kim, *Inorg. Chem.* **1985**, *24*, 3712–3714; d) M. P. Suh, W. Shin, H. Kim, C. H. Koo, *Inorg. Chem.* **1987**, *26*, 1846–1852; e) M. P. Suh, S.-G. Kangl, *Inorg. Chem.* **1988**, *27*, 2544–2546; f) T. Kojima, T. Usui, T. Tanase, M. Yashiro, S. Yoshikawa, R. Kuroda, S. Yano, M. Hidai, *Inorg. Chem.* **1990**, *29*, 446–450; g) T. Kojima, R. Kuroda, S. Yano, M. Hidaif, *Inorg. Chem.* **1991**, *30*, 3580–3582; h) L. Fabbrizzi, A. M. M. Lanfredi, P. Pallavicini, A. Perotti, A. Taglietti, F. Ugozzoli, *J. Chem. Soc. Dalton Trans.* **1991**, 3263–3269; i) T. Kojima, T. Usui, A. Shimada, M. Yashiro, T. Tanase, R. Yoshioka, R. Kuroda, S. Yano, M. Hidai, M. Kato, K. Kobayashi, T. Sakurai, S. Yoshikawa, *Inorg. Chem.* **1991**, *30*, 4535; j) M. P. Suh, B. Y. Shim, T.-S. Yoon, *Inorg. Chem.* **1994**, *33*, 5509–5514; k) P. V. Bernhardt, P. C. Sharpe, *Inorg. Chem.* **2000**, *39*, 2020–2025; l) P. Bernhardt, J. C. Hetherington, *J. Chem. Soc. Dalton Trans.* **1996**, 4325–4330.
[17] a) M. D. Fletcher, M. M. Campbell, *Chem. Rev.* **1998**, *98*, 763–795; b) W. J. N. Meester, J. H. van Maarseveen, H. E. Schoemaker, H. Hiemstra, F. P. J. T. Rutjes, *Eur. J. Org. Chem.* **2003**, 2519.
[18] M. Suchý, R. H. E. Hudson, *Eur. J. Org. Chem.* **2008**, 4847–4865.
[19] a) P. Surdy, P. Rubini, N. Buzás, B. Henry, L. Pellerito, T. Gajda, *Inorg. Chem.* **1999**, *38*, 346–352; b) F. Gharib, M. H. Fekri, *J. Solution Chem.* **2003**, *32*, 855–863.
[20] C. M. Loudon, M. R. Almond, J. N. Jacob, *J. Am. Chem. Soc.* **1981**, *103*, 4508.
[21] F. Moriya, K. Maklno, N. Suzukl, S. Rokushlka, H. Hatano, *J. Phys. Chem.* **1980**, *84*, 3085–3090.
[22] a) L. R. Gahan, T. W. Hambley, A. M. Sargeson, M. R. Snow, *Inorg. Chem.* **1982**, *21*, 2699–2706; b) M. P. Suh, W. Shin, S.-G. Kang, M. S. Lah, T.-M. Chung, *Inorg. Chem.* **1989**, *28*, 1602–1605.
[23] R. W. Alder, T. M. G. Carniero, R. W. Mowlam, A. G. Orpen, P. A. Petillo, D. J. Vachon, G. R. Weisman, J. M. White, *J. Chem. Soc. Perkin Trans. 2* **1999**, 589–599.
[24] a) Y. Mo, *Nat. Chem.* **2010**, *2*, 666–671; b) O. Takahashi, K. Yamasaki, Y. Kohno, K. Ueda, H. Suezawa, M. Nishio, *Carbohydr. Res.* **2009**, *344*, 1225–1229; c) S. Chandrasekhar, *ARKIVOC* **2005**, 37–66.
[25] a) M. K. Kesharwani, W. Thiel, B. Ganguly, *J. Phys. Chem. A* **2010**, *114*, 10684–10693; b) B. Ganguly, B. Fuchs, *J. Org. Chem.* **1997**, *62*, 8892–8901.
[26] a) W. De, W. J. Horrocks, D. R. Sudnick, *J. Am. Chem. Soc.* **1979**, *101*, 334–340; b) R. M. Supkowski, W. De, W. J. Horrocks, *Inorg. Chim. Acta* **2002**, *340*, 44–48; c) A. Beeby, I. M. Clarkson, R. S. Dickins, S. Faulkner, D. Parker, L. Royle, A. S. deSousa, J. A. G. Williams, M. Woods, *J. Chem. Soc. Perkin Trans. 2* **1999**, 493–502.
[27] N. Graeppi, D. H. Powell, G. Laurenczy, L. Zékány, A. E. Merbach, *Inorg. Chim. Acta* **1995**, *235*, 311–326.
[28] a) P. H. Fries, E. Belorizky, *J. Chem. Phys.* **2005**, *123*, 124510; b) P. Miéville, H. Jaccard, F. Reviriego, R. Tripier, L. Helm, *Dalton Trans.* **2011**, *40*, 4260–4267.
[29] D. H. Powell, O. M. N. Dhubhghaill, D. Pubanz, L. Helm, Y. S. Lebedev, W. Schlaepfer, A. E. Merbach, *J. Am. Chem. Soc.* **1996**, *118*, 9333–9346.
[30] B. Yoo, M. D. Pagel, *J. Am. Chem. Soc.* **2006**, *128*, 14032–14033.

[31] a) S. Forsén, R. A. Hoffman, *J. Chem. Phys.* **1963**, *39*, 2892–2901; b) S. Forsén, R. A. Hoffman, *J. Chem. Phys.* **1964**, *40*, 1189–1196.
[32] M. T. McMahon, A. A. Gilad, J. Zhou, P. Z. Sun, J. W. M. Bulte, P. C. M. vanZijl, *Magn. Reson. Med.* **2006**, *55*, 836–847.
[33] S. Zhang, P. Winter, K. Wu, A. D. Sherry, *J. Am. Chem. Soc.* **2001**, *123*, 1517–1518.
[34] W. T. Dixon, J. Ren, A. J. M. Lubag, J. Ratnakar, E. Vinogradov, I. Hancu, R. E. Lenkinski, A. D. Sherry, *Magn. Reson. Med.* **2010**, *63*, 625–632.
[35] S. Zhang, L. Michaudet, S. Burgess, A. D. Sherry, *Angew. Chem.* **2002**, *114*, 1999–2001; *Angew. Chem. Int. Ed.* **2002**, *41*, 1919–1921.
[36] E. Liepinsh, G. Otting, *Magn. Reson. Med.* **1996**, *35*, 30–42.
[37] G. Liu, Y. Li, M. D. Pagel, *Magn. Reson. Med.* **2007**, *58*, 1249–1256.
[38] B. Yoo, M. S. Raam, R. M. Rosenblum, M. D. Pagel, *Contrast Media Mol. Imaging* **2007**, *2*, 189–198.
[39] S. Aime, A. Barge, D. D. Castelli, F. Fedeli, A. Mortillaro, F. U. Nielsen, E. Terreno, *Magn. Reson. Med.* **2002**, *47*, 639–648.
[40] R. L. Vold, J. S. Waugh, M. P. Klein, D. E. Phelps, *J. Chem. Phys.* **1968**, *48*, 3831.
[41] S. Meiboom, D. Gill, *Rev. Sci. Instrum.* **1958**, *29*, 688–691.
[42] A. D. Hugi, L. Helm, A. E. Merbach, *Helv. Chim. Acta* **1985**, *68*, 508–521.
[43] D. S. Raiford, C. L. Fisk, E. D. Becker, *Anal. Chem.* **1979**, *51*, 2050–2051.
[44] H. M. Irving, M. G. Miles, L. Pettit, *Anal. Chim. Acta* **1967**, *38*, 475–488.
[45] L. Zékány, I. Nagypál in *Computation Methods for Determination of Formation Constants* (Ed.: D. J. Leggett), Plenum, New York, **1985**, p. 291.

Received: June 10, 2011
Revised: October 21, 2011
Published online: December 28, 2011

